

Phase Crossover induced by Dynamical Many Body Localization in Periodically Driven Long-Range Spin Systems

Mahbub Rahaman,¹ Takashi Mori,² and Analabha Roy¹

¹Department of Physics, The University of Burdwan, Golapbag, Bardhaman - 713 104, India

²RIKEN CEMS, 2-1 Hirosawa, Wako, Saitama, 351-0198, Japan

Dynamical many-body freezing occurs in periodic transverse field-driven integrable quantum spin systems. Under resonance conditions, quantum dynamics causes practically infinite hysteresis in the drive response, maintaining its starting value. We extended this to non-integrable many body systems by reducing the Hamiltonian symmetries through a power-law dependence in spin exchange energy, $J_{ij} = 1/|i - j|^\beta$. The dynamics of the integrable short-range Transverse Field Ising Model (TFIM) and non-integrable long-range Lipkin Meshkov-Glick (LMG) models were investigated. In the LMG, the resonance conditions in the driving field suppresses the heating postulated by the *Eigenstate Thermalization Hypothesis* (ETH) by inducing *Dynamical Many Body Localization*, or DMBL. This is in contrast to Many Body Localization (MBL), which requires disorder to suppress ETH. DMBL has been validated by the Inverse Participation Ratio (IPR) of the quasi-stationary Floquet modes. While TFIM has IPR localization for all drive parameters, the LMG exhibits high-frequency localization only at the resonances. IPR localization in the LMG deteriorates with an inverse system size law at lower frequencies, which indicates heating to infinite temperature. Furthermore, adiabatically increasing frequency and amplitude from low values raises the Floquet state IPR in the LMG from nearly zero to unity, indicating a phase crossover. This occurrence enables a future technique to construct an MBL engine in clean systems that can be cycled by adjusting drive parameters only.

Keywords: Dynamical localization, Thermalization, Phase Crossover

Periodically driven Quantum Many Body Systems can, under certain conditions, experience Dynamical Many-Body Freezing (DMF) when dynamical hysteresis stops observables from reaching their diagonal averaged values and thermalizing to infinite temperature [1–3].

Under certain resonance conditions in the drive parameters, DMF can cause the response to ‘freeze’ completely to its initial value at all times. This arises as a consequence of additional approximate symmetries that occur at resonance. DMF has been demonstrated via the Rotating Wave Approximation (RWA) in the driven TFIM with nearest-neighbour interactions [4] and is shown to be protected when translational invariance is explicitly broken (say, by disorder) [5, 6].

The utilization of Floquet theory simplifies the analysis of time-periodic systems. For closed quantum systems governed by the time-dependent Schrödinger equation, the *Floquet Hamiltonian* allows for a mapping of the time-dependent dynamics into the dynamics of a time-independent effective Hamiltonian, provided the system is strobed at integer multiples of the time period of the drive. The time independent eigenstates of the effective Hamiltonian correspond to quasi-stationary *Floquet Modes* of the original Hamiltonian. The temporal progression of the system comes from phase coefficients that capture the dynamics [7, 8].

Any sufficiently complex non-integrable Many Body System is expected to thermalize according to the

Eigenstate Thermalization Hypothesis (ETH) despite the fact that closed quantum dynamics preserves the memory of the initial state of the system. This arises due to the properties of the matrix elements of observables in typical states[9]. The ETH can be readily adapted to time-periodic systems using Floquet theory (the Floquet-ETH, or FETH). Nonetheless, the conditions for ETH to hold are not particularly strong, and the density matrix of the system can fail to approach one that is described by a thermal expression. In such cases, the system is said to undergo *Many Body Localization* (MBL). Thermal systems must conduct because they exchange energy and particles internally during thermalization. Thus, insulating systems can be naturally athermal; Many Body Localization is a well-studied case [10]. This phenomenon is stable against local perturbations, and constitutes an exotic state of matter with far-reaching implications in theoretical physics, as well as in practical applications[11].

The addition of disorder has been identified as a crucial component in the onset of MBL. In that case, thermalization is prevented by disorder-induced localization. Nonetheless, alternative approaches to MBL in strongly interacting disorder-free systems [12–14], inhomogeneous systems [15–18], and by inducing disorder in the emergent physics [19] and by other effective means [17] (albeit with strong finite-size effects), have been reported. An alternative approach to realizing MBL in disorder-free homogeneous many-body systems involve *Floquet Engineering*, where a time-

See an-
notation.

68 periodic drive is introduced, and the drive parameters
 69 tuned to introduce a clustering of quasistationary en-
 70 ergies in a manner similar to localization[9].

71 In this article, we propose that additional approxi-
 72 mate symmetries can be Floquet engineered in quan-
 73 tum many body systems with lower symmetry than the
 74 TFIM, such as those with long range interactions. We
 75 use the fact that emergent approximate symmetries
 76 can be engineered in Floquet systems and apply it
 77 to long-range interactions. This results in both DMF
 78 and MBL occurring simultaneously at resonant val-
 79 ues of the drive parameters, and complete thermal be-
 80 haviour at other values. This phenomenon is distinct
 81 from DMF in the TFIM, since clean TFIM systems, be-
 82 ing integrable, never thermalize..

See an-
notation

83 To demonstrate the onset of MBL, we investigate
 84 the driven Lipkin-Meshkov-Glick (LMG) model[20-
 85 25], a long-range system that extends the nearest
 86 neighbour interactions in the TFIM to all-to-all inter-
 87 actions. [26-28] that is a special case of the more gen-
 88 eral Curie-Weiss model, wherein the nearest neigh-
 89 bour exchange in the TFIM is extended to longer
 90 ranges with a power law dependence, $J_{ij} \sim 1/|i-j|^\beta$
 91 . Setting $\beta = \infty$ recovers the TFIM, and setting $\beta = 0$
 92 yields the LMG model. We have recovered the onset
 93 of DMF in this system and have supported our result
 94 with numerical simulations.

95 In addition, we compare the degree of localization
 96 of the quasi-stationary Floquet modes in both limits
 97 of β in the LMG model with the TFIM. In order to
 98 do so, we look at the Inverse Participation Ratio (IPR)
 99 of the Floquet modes in the representation given by
 100 the eigenstates of the symmetry-breaking field. The
 101 IPR, closely related to the concept of quantum purity,
 102 is defined as the formal sum of the square of the den-
 103 sity in some physically meaningful space or represen-
 104 tation. A high IPR of a stationary state denotes low
 105 participation in most of the representation, and a low
 106 IPR distributes participation uniformly across the rep-
 107 resentation, leading to ergodic dynamics[29]. Thus,
 108 IPR [30] is a useful tool for witnessing MBL of a quan-
 109 tum system. For an MBL system, the IPR is unity,
 110 and it scales inversely with the system size number
 111 of spins when it is thermally distributed [31].

112 In the first section of this paper, we present all es-
 113 sential theoretical frameworks. Our results for the
 114 LMG model are presented next in section II. In that
 115 section, we have used the Rotating Wave Approx-
 116 imation (RWA) [32], where only the slowest rotating
 117 terms in the Fourier expansion of the Hamiltonian in
 118 a frame co-rotating with the symmetry breaking drive
 119 field are retained. In addition, we have the obtained
 120 analytical expressions for numerical simulations of the
 121 Floquet modes and their IPR. They are used to probe
 122 the system dynamics in the high and low-frequency

124 domains at both limits of β . In section III we have
 125 used phase space plots to contrast the low and high
 126 frequency limits of the LMG model in the thermody-
 127 namic limit by mapping it to an equivalent classical
 128 Hamiltonian system. Finally, in section IV, we have
 129 looked at numerical computations of the IPR of the
 130 Floquet modes for different values of the drive pa-
 131 rameters, well beyond those that allow for the RWA.
 132 We observed that, if the system is driven by an adia-
 133 batically increasing drive frequency from low to high
 134 limit while remaining in the resonance region, a sharp
 135 crossover from a thermal to an MBL phase occurs. We
 136 conclude with discussions and outlook.

I. BACKGROUND

138 The Eigenstate Thermalization Hypothesis (ETH) is
 139 a series of conjectures that allows for the thermaliza-
 140 tion of an isolated quantum many body system. The
 141 state of the system, $|\psi(t)\rangle$, evolves according to the
 142 Schrödinger equation $\hat{H}|\psi(t)\rangle = i\frac{\partial}{\partial t}|\psi\rangle$. The Hamilto-
 143 nian \hat{H} is assumed to be non-integrable, in that it lacks
 144 an extensive number of local additive conserved quan-
 145 tities, that is to say, there are no set of observables
 146 \hat{O}_s such that $\hat{H} = \sum_s \hat{O}_s$ for any extensive index s .
 147 Here, the \hat{O}_s constitute an arbitrary CSCO (complete
 148 set of commuting observables) that are local, having
 149 sub-extensive support in the system size. In addition,
 150 we postulate the existence of an equivalent Hamilto-
 151 nian \hat{H}_{eq} for every Hamiltonian \hat{H} as well as an "equi-
 152 librium" value A_{eq} for every observable \hat{A} , such that

$$A_{eq}(E) \equiv \frac{\text{Tr}(\hat{A}e^{-\beta\hat{H}_{eq}})}{\text{Tr}(e^{-\beta\hat{H}_{eq}})}, \quad (1)$$

153 where $E = \langle\psi(t)|\hat{H}|\psi(t)\rangle$ is the conserved energy of
 154 the system, and $\beta = 1/(k_B T)$ is the inverse tempera-
 155 ture, H_{eq} is an effective Hamiltonian that captures the
 156 long-time average dynamics of the system, and k_B is
 157 the Boltzmann constant.

Suggestions
for
rewriting
this?

158 To put it simply, ETH proposes that this many-
 159 body Hamiltonian undergoes thermalization as seen
 160 in the long-time averages of observables, with the
 161 eigenstates bearing resemblance to thermal states.
 162 The aforementioned hypothesis serves as a valuable
 163 instrument for comprehending the conduct of stim-
 164 ulated quantum systems and their correlation with
 165 thermal equilibrium. This assertion can be justified
 166 by examining the expectation value of an observable
 167 \hat{A} as it evolves under the Schrödinger equation. To
 168 see this, we first expand the state of the system $|\psi(t)\rangle$

as:

$$|\psi(t)\rangle = \sum_m c_m(t) |m(0)\rangle,$$

where $|m(0)\rangle$ represents the eigenstates of $\hat{H}(0)$ with energy E_m . The coefficients $c_m(t)$ describe the time-dependent amplitude of the expansion. Plugging these expansions into the expression for the expectation value, we obtain the long-time average of the expectation value [33]:

$$\overline{\langle \hat{A}(t) \rangle} = \sum_{m,k} \overline{c_m^*(t)c_k(t)} \langle m(0) | \hat{A} | k(0) \rangle, \quad (2)$$

where the overline indicates the following operation for any time-dependent quantity $\mathcal{O}(t)$,

$$\overline{\mathcal{O}} \equiv \lim_{t \rightarrow \infty} \frac{1}{t} \int_0^t d\tau \mathcal{O}(\tau). \quad (3)$$

~~Had the system been integrable, the large number of conserved quantities would restrict mixing between the states during unitary evolution. In the non-integrable case, the system explores the entire Hilbert space spanned by eigenstates with eigenvalues close to E more or less uniformly. In that case, the matrix elements $\langle m(0) | \hat{A} | k(0) \rangle$ are said to satisfy the Srednicki ansatz [34, 35]:~~

$$\begin{aligned} \langle m(0) | \hat{A} | k(0) \rangle &\approx A_{eq} \left(\frac{E_m + E_k}{2} \right) \delta_{mk} + \\ &e^{-\frac{1}{2}S\left(\frac{E_m+E_k}{2}\right)} f \left(\frac{E_m + E_k}{2}, E_m - E_k \right) R_{mk}. \end{aligned} \quad (4)$$

Here, S is the thermodynamic entropy and R_{mk} are elements of a random matrix with vanishing mean and unit variance. What this means for the ensuing dynamics is that the system explores the accessible Hilbert space uniformly, and the matrix elements $\langle m(0) | \hat{A}(t) | k(0) \rangle$ become indistinguishable for most pairs of m and k . Applying this ansatz and taking the thermodynamic limit by ignoring terms $\mathcal{O}(e^{-S/2})$, the expression for the expectation value becomes:

$$\begin{aligned} \overline{\langle \hat{A}(t) \rangle} &\approx \sum_m \overline{|c_m(t)|^2} A_{eq}(E_m) \\ &\approx A_{eq}(E) \sum_m \overline{|c_m(t)|^2} = A_{eq}(E), \end{aligned}$$

where, in the last step, we utilized the fact that A_{eq} is a smooth function, and that the states with energies far from E have $|c_m(t)|^2 \approx 0$. Therefore, in the limit of large systems the expectation value of an observable \hat{A} is approximately equal to the thermal expectation value A_{eq} . This is the essence of the ETH, which suggests that individual eigenstates of a quantum system

can be described by statistical mechanics in the long-time limit.

We now generalize the ETH to non-integrable many body systems that are closed, but not isolated. In that case, it is possible to impart a periodic time-dependence on the Hamiltonian while still ensuring unitary evolution. If the time period of the drive is T , and the corresponding drive frequency $\omega \equiv 2\pi/T$, the Floquet theorem states that the solutions to the Schrödinger equation can be written as $|\psi(t)\rangle = e^{-i\epsilon t/\hbar} |\phi(t)\rangle$, where the $|\phi(t)\rangle$ are T -periodic states called *Floquet Modes*, the corresponding $\epsilon \in \mathbb{R}$, are called *quasienergies*. Quasienergy values are not unique, and can be made to be bounded within a Floquet photon Brillouin zone, viz. a range $[-\omega/2, \omega/2]$ [36, 37]. As a consequence, the unitary evolution operator can be split into two parts as follows [38].

$$U(t) = e^{-i\hat{K}_F(t)} e^{-i\hat{H}_F t}. \quad (5)$$

Here, the micromotion operator $\hat{K}_F(t)$ is time-periodic in T , with $\hat{K}_F(0) = 0$, and the Floquet Hamiltonian $\hat{H}_F = \hat{H}(t) - i \frac{\partial}{\partial t} \Big|_{t=T}$

$$\hat{H}_F = e^{i\hat{K}_F(t)} [\hat{H}(t) - i\partial_t] e^{-i\hat{K}_F(t)}. \quad (6)$$

Thus, if the system is strobed at integer multiples of T only, then the unitary evolution matches that of a time independent Hamiltonian H_F . This can capture most of the exact dynamics at large frequencies.

In such systems, the Floquet Eigenstate Thermalization Hypothesis (FETH) posits that, subject to specific conditions and in the context of a system of significant size, the Floquet modes themselves exhibit thermal state-like behavior, i.e., $\hat{H}_{eq} \approx \hat{H}_F$ in eqn 1. However, in contrast to the isolated systems, the loss of energy conservation allows for the mixing of all Floquet modes in the ensuing dynamics, not just those with quasienergies near E . Were this to actually happen in the ensuing dynamics, it can be reconciled with ETH [39] by ensuring that $\beta = 0$ in eq 1. It can be reconciled with ETH by ensuring that the RHS of eqn 1 is independent of β , i.e., an infinite temperature ensemble [39]. In other words, the nonequilibrium steady state of the system tends to an infinite temperature, maximum entropy density matrix.

However, drive parameters like amplitude, frequency, and duty-cycle strongly affect the structure of the Floquet modes $|\phi\rangle$. Thus, they can be engineered to prevent the kind of full mixing that would lead to infinite temperatures, manifesting suppression of thermalization dynamically. Thus, this type of Floquet Engineering can produce *Dynamical Many Body Localization* (DMBL), where the system fails to reach thermal equilibrium and remains localized,

possibly near its initial state, even at large times. This paradigm seems similar to standard Many-Body Localization[40, 41], where disorder, locality, and integrability can cause athermality via breakdown in the Srednicki ansatz. However, DMBL is a ~~purely dynamical phenomenon~~ stems from periodic driving, and thus can occur regardless of disorder, locality of observables, or system integrability, all of which have been studied for MBL onset [42–44].

Integrable Many Body systems do not exhibit thermalization. When subjected to time-periodic drives, Floquet engineering allows for the introduction of additional approximate conserved quantities that dynamically suppress the evolution of certain observables by hysteresis. This type of *freezing* of response has been shown in integrable systems [6]. A paradigmatic example is the driven Transverse Field Ising model (TFIM) in one dimension [45]. The Hamiltonian is given by

$$\hat{H}(t) = \hat{H}_0 + h_z(t) \hat{H}_1, \quad (6)$$

$$\hat{H}_0 = -\frac{1}{2} \sum_{i=1}^N \sigma_i^x \sigma_{i+1}^x, \quad (7)$$

$$\hat{H}_1 = -\frac{1}{2} \sum_{i=1}^N \sigma_i^z. \quad (8)$$

Here, the undriven Hamiltonian \hat{H}_0 consists of nearest-neighbour interactions between N number of spin-1/2 particles on a one-dimensional spin network. The transverse field is denoted by \hat{H}_1 , and is being varied by a time-periodic and harmonic signal $h_z(t) = h_0 + h \cos \omega t$, yielding a time period $T = 2\pi/\omega$ with amplitude h , drive frequency ω , and d.c. field h_0 . This Hamiltonian can be readily transformed into a spinless pseudo-fermionic system via the Jordan-Wigner transformation [4]. When written in momentum space spanned by spinors $\psi_k = (c_{-k}, c_k^\dagger)^T$ of fermions at momentum k created (annihilated) by operators c_k^\dagger (c_k), the effective Hamiltonian

$$H(t) = \sum_{(k,-k)-\text{pairs}} \psi_k^\dagger \left[\left(f_k - h_z(t) \right) \tau_z + \tau_x \Delta_k \right] \psi_k, \quad (9)$$

where $f_k = \cos k$, $\Delta_k = \sin k$, τ_{xyz} are the three Pauli Matrices, and the sum is over distinct $(k, -k)$ Cooper Pairs. We can transform our system to a frame that rotates with the time-varying symmetry-breaking field. This is achieved by the means of the unitary transformation operator

$$U(t) = \prod_k U_k(t) \quad (10)$$

$$U_k(t) = \exp \left\{ \left[\frac{i\hbar}{\omega} \sin \omega t \right] \tau_z \right\}.$$

The resulting transformed Hamiltonian $H'(t) = U^\dagger(t) H(t) U(t) - iU^\dagger(t) \partial_t U(t)$ simplifies to

$$H'(t) = \sum_{(k,-k)-\text{pairs}} \psi_k^\dagger \left[\tau_z f_k + \tau_x \cos(\eta \sin \omega t) + \tau_y \sin(\eta \sin \omega t) \right] \psi_k, \quad (11)$$

where we defined $\eta = 2h/\omega$. Using the Jacobi-Anger formula [46]

$$e^{i\eta \sin \omega t} = \sum_{n=-\infty}^{\infty} J_n(\eta) e^{in\omega t}, \quad (12)$$

where $J_n(\eta)$ are Bessel Functions, the transformed Hamiltonian simplifies to

$$H'(t) = \sum_{(k,-k)-\text{pairs}} \psi_k^\dagger \left\{ \tau_z f_k + 2\tau_x \Delta_k \sum_{n \geq 0} J_{2n}(\eta) \cos(2n\omega t) - 2\tau_y \Delta_k \sum_{n \geq 0} J_{2n+1}(\eta) \sin[(2n+1)\omega t] \right\} \psi_k. \quad (13)$$

In the frequency regime $\omega \gg f_k$, the long-time average $H^{RWA} \equiv \lim_{n \rightarrow \infty} \frac{1}{nT} \int_0^{nT} dt H'(t)$ can serve as a suitable approximation for $H'(t)$. This approximation, known as the *Rotated Wave Approximation* (RWA), eliminates the oscillating modes and results in an effective Hamiltonian that is independent of time,

$$H^{RWA} = \sum_{(k,-k)-\text{pairs}} \psi_k^\dagger \left[f_k \tau_z + 2J_0(\eta) \Delta_k \tau_x \right] \psi_k. \quad (14)$$

It is evident that by manipulating the drive parameters, specifically the amplitude denoted by h and the frequency denoted by ω , in a manner such that η is positioned on a root of $J_0(\eta)$, the fermion number can be conserved to a significant extent at this particular resonance. Consequently, it is feasible to exercise direct control over H^{RWA} , resulting in a comprehensive suppression of the dynamics of otherwise responsive observables.

This phenomenon is highly general in nature, and can be readily adapted to non-integrable systems. In such cases, freezing has the additional effect of inducing DMBL, suppressing thermalization to infinite temperatures. Numerical quantification of localization of a specific (quasi) stationary state in a physically significant representation can be achieved through the computation of the *Inverse Participation Ratio* (IPR). The IPR is generally defined as the formal sum over

the square of the local density in a physically meaningful space. [47–50] In the single particle case, the IPR, for a state $|\psi\rangle$ can be written as

$$\phi_{IPR} \equiv \int d\mathbf{x} |\langle \mathbf{x} | \psi \rangle|^4.$$

²⁶⁴ This definition can be generalized applied to obtain
²⁶⁵ the IPR of a state $|\phi\rangle$ in a representation given by any
²⁶⁶ complete orthonormal single particle basis $|m\rangle$ as

$$\phi_{IPR} \equiv \sum_m |\langle m | \psi \rangle|^4. \quad (15)$$

²⁶⁷ The smallest value of the IPR corresponds to a fully
²⁶⁸ de-localized state, $\psi(x) = 1/\sqrt{N}$ for a system of size
²⁶⁹ N [50, 51]. Values of the IPR close to unity correspond
²⁷⁰ to localized states [52]. For a periodically driven sys-
²⁷¹ tem, we look at the IPR of the quasi-stationary Floquet
²⁷² modes at $t = T$, where $t = 2\pi/\omega$ for drive frequency ω .
²⁷³ In the TFIM model, equation 14 indicates that, at reso-
²⁷⁴ nance, when $J_0(\eta) = 0$, the Floquet modes are approx-
²⁷⁵ imately given by the fermionic Fock states, which have
²⁷⁶ a trivially unit IPR in the representation of the eigen-
²⁷⁷ modes of the transverse field \hat{H}_1 in equation 6. Here, a
²⁷⁸ particular Floquet mode can be decomposed into a di-
²⁷⁹ rect product of cooper-pair states as $|\phi\rangle = \prod_{k,-k} |\phi_k^n\rangle$.
²⁸⁰ In the RWA limit and at resonance, $|\phi_k^n\rangle$ has values of
²⁸¹ $|0\rangle, |k, -k\rangle$ for two values of $n = 0, 1$ respectively. We
²⁸² define the reduced IPR of $|\phi_k^n\rangle \forall k$ to be

$$\phi_{IPR}^{(n)}(k) = |\langle 0 | \phi_k^n \rangle|^4 + |\langle +k, -k | \phi_k^n \rangle|^4, \quad (16)$$

²⁸³ where $n = 0, 1$. In the RWA limit and at resonance ,
²⁸⁴ this quantity is unity, indicating very low participation
²⁸⁵ and the onset of freezing. Figure 1 shows results from
²⁸⁶ numerically simulating the TFIM dynamics. The re-
²⁸⁷duced IPR for a particular Floquet mode recovered by
²⁸⁸ simulating the exact Schrödinger dynamics over a sin-
²⁸⁹gle time period of the drive, and plotted as a function
²⁹⁰ of momentum k for different η 's. At resonance, when
²⁹¹ η lies at the root of the Bessel function $J_0(\eta)$, the IPR
²⁹² is exactly nearly unity for all momenta. Outside this
²⁹³ resonance, the IPR is unity only for some momenta
²⁹⁴ because the effective Hamiltonian is perfect diagonal
²⁹⁵ at $k \in \{-\pi, 0, \pi\}$ as can be seen in the cross-sectional
²⁹⁶ plots of figure 1. As we move away from the resonance
²⁹⁷ point, IPR reduces from unity. However, as the TFIM
²⁹⁸ is an integrable spin model, the IPR never drops to a
²⁹⁹ value that is small enough to indicate thermalization.
³⁰⁰ At low frequencies, RWA fails due to the unavailability
³⁰¹ of zero off-diagonal terms in the effective transformed
³⁰² Hamiltonian, as well as the absence of integrability
³⁰³ breaking terms to counteract the off diagonal terms.
³⁰⁴ Consequently, the IPR remains quite high (~ 0.5) even
³⁰⁵ at the resonance point as can be seen figure 1. At low
³⁰⁶ frequency, this is valid for all momentum and parame-
³⁰⁷ ter η , see figure 2.

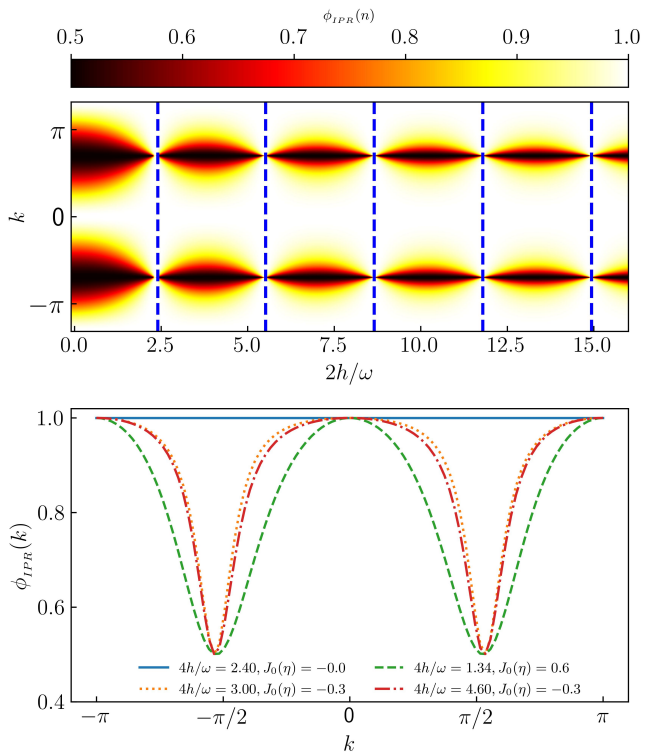


FIG. 1. Reduced IPR (defined in equation 16) for one of the two Floquet modes obtained from the exact dynamics of the TFIM for size $N = 100$ and $\omega = 90$ for the entire Brillouin zone (top panel, ordinate) and a few drive amplitudes (top panel, abscissa). The dashed lines (top panel) indicate the roots of $J_0(\eta)$. The bottom panel shows cross-sections for four different chosen amplitudes.

³¹⁰ Because the dependence of observable expectations
³¹¹ on the eigenstates is always fairly strong for inte-
³¹² grable systems like the TFIM, such systems will never
³¹³ exhibit any kind of thermal behaviour unless integra-
³¹⁴ bility breaking terms (such as strong disorder) are in-
³¹⁵ cluded [6]. As a result, it is not physically meaningful
³¹⁶ to refer to the unit IPR region as "Many Body Localiza-
³¹⁷ tion", because the parameter space lacks a thermal-
³¹⁸ ized region to contrast with this state. The type of Flo-
³¹⁹ quet Engineering described above, on the other hand,
³²⁰ can be easily applied to a broad class of nonintegrable
³²¹ systems where FETH is expected to hold in certain re-
³²² gions. Long-range spin systems, in particular, where
³²³ the exchange energies between far-off spins are taken
³²⁴ into account in the model Hamiltonian, are good can-
³²⁵ didates because they are known to thermalize when
³²⁶ driven with low frequencies [53].

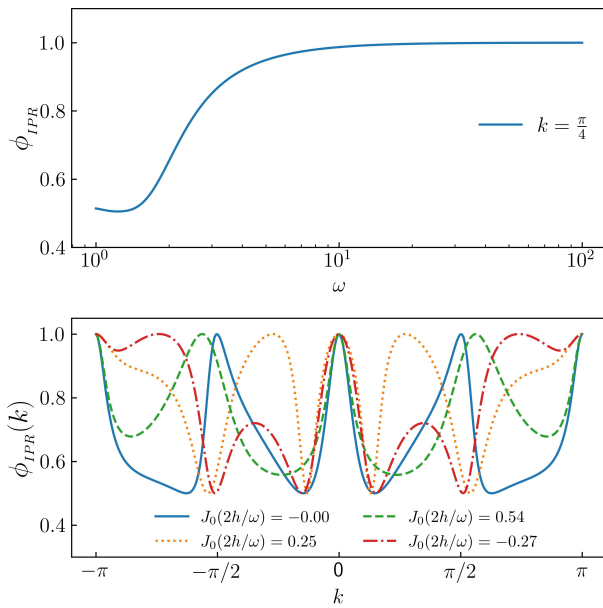


FIG. 2. Reduced IPR obtained by adiabatically increasing ω (top panel abscissa) for one the floquet mode obtained from equation 16 at the root of $J_0(\eta)$ for $N = 500$. IPR is ~ 0.5 (localized yet not fully freezing) upto $\omega \sim 2$, after that, smoothly increased to unity (fully localized and freezing) at higher $\omega \geq 10$ (top panel, ordinate). At bottom panel cross-sections for four chosen amplitudes at $\omega = 2$ are plotted for a brillouin zone (abscissa) with corresponding reduced IPRs (ordinate).

327 II. LONG RANGE INTERACTIONS: THE LIPKIN 328 MESHKOV GLICK MODEL:

329 The periodically driven Curie-Weiss Lipkin Meshkov
330 Glick (LMG) model [20, 54] for N long-range spins is
331 described by the Hamiltonian

$$\hat{H}(t) = \hat{H}_0 + [h \cos(\omega t) + h_0] \hat{H}_1. \quad (17)$$

332 Here, the undriven part \hat{H}_0 and the driven part \hat{H}_1 are,
333 respectively,

$$\begin{aligned} \hat{H}_0 &= \frac{2}{N-1} \sum_{ij} \hat{\sigma}_i^z \hat{\sigma}_j^z, \\ \hat{H}_1 &= \sum_{i=1}^N \hat{\sigma}_i^x. \end{aligned} \quad (18)$$

The Kac-norm of $2/(N-1)$ arises from the choice to maintain the extensivity of the interaction energy. The Hamiltonian in equation 17 commutes with $P_{ij} \equiv$

$\frac{1}{2}(1 + \vec{\sigma}_i \cdot \vec{\sigma}_j)$. In addition, it also commutes with the total angular momentum $S^2 = |\vec{S}|^2$, where $\vec{S} = S^x \hat{x} + S^y \hat{y} + S^z \hat{z} \equiv \frac{1}{2} \sum_i \vec{\sigma}_i$. We now choose to populate the system in a state with $S^2 = \frac{N}{2} \left(\frac{N}{2} + 1 \right)$. In that case, the dynamics remains invariant in the $N+1$ -dimensional space spanned by the common eigenstates of P_{ij} , $|S|^2$ and S_z ; the so-called *Totally Symmetric Subspace*, or TSS [55]. Let the eigenvalues of S^z in the TSS be s_n , and the eigenvectors be $|s_n\rangle$. Here, $s_n = -\frac{1}{2} + \frac{n}{N}$ and the index $n = 0(1)N$ has $N+1$ values. The dynamics is restricted to this invariant subspace, wherein the matrix elements of the Hamiltonian are given by

$$\begin{aligned} \langle s_i | \hat{H}_0 | s_j \rangle &= -\frac{4}{N-1} s_i^2 \delta_{ij}, \\ \langle s_i | \hat{H}_1 | s_j \rangle &= \left[\sqrt{\frac{N}{2} \left(\frac{N}{2} + 1 \right) - N s_i (N s_{i+1})} \delta_{i+1,j} \right. \\ &\quad \left. + \sqrt{\frac{N}{2} \left(\frac{N}{2} + 1 \right) - N s_i (N s_{i-1})} \delta_{i-1,j} \right]. \end{aligned} \quad (19)$$

These allow for a numerical representation of the Hamiltonian in the TSS.

Next, we transform the Hamiltonian to the rotated frame given by the operator

$$\hat{U}(t) = \exp \left[i \frac{h}{\omega} \sin(\omega t) \hat{H}_1 \right]. \quad (20)$$

This is analogous to the rotation performed for the TFIM in eqns 10 and 11. Defining $\tau = \frac{h}{\omega} \sin \omega t$, we use the fact that $\hat{H}_1 = 2S^x$, as well as the following identity obtained by using the Baker-Campbell-Hausdorff formula,

$$e^{i2\tau \hat{S}^x} \hat{S}^z e^{-i2\tau \hat{S}^x} = \hat{S}^z \cos(2\tau) + \hat{S}^y \sin(2\tau), \quad (21)$$

to simplify the transformed Hamiltonian $\tilde{H}(t) = \hat{U}^\dagger(t) \hat{H}(t) \hat{U}(t) - \hat{U}^\dagger(t) \partial_t \hat{U}(t)$, yielding

$$\begin{aligned} \tilde{H}(t) &= -\frac{1}{N-1} \left[(S^z)^2 (1 + \cos 4\tau) + (S^y)^2 (1 - \cos 4\tau) \right. \\ &\quad \left. + \{S^y, S^z\} \sin 4\tau \right] - 2h_0 S^x. \end{aligned} \quad (22)$$

Next, we define $\eta \equiv 4h/\omega$ and use the Jacobi-Anger formula in eqn 12 to expand $\tilde{H}(t)$. This yields

$$\tilde{H}(t) = -\frac{\hat{S}^2}{N-1} + \frac{(\hat{S}^x)^2}{N-1} - 2h_0\hat{S}^x - \frac{J_0(\eta)}{N-1} \left[(\hat{S}^z)^2 - (\hat{S}^y)^2 \right] - \frac{2}{N-1} \left[(\hat{S}^z)^2 - (\hat{S}^y)^2 \right] \sum_{k=1}^{\infty} J_{2k}(\eta) \cos(2k\omega t) - \frac{2}{N-1} \{ \hat{S}^y, \hat{S}^z \} \sum_{k=1}^{\infty} J_{2k-1}(\eta) \sin[(2k-1)\omega t]. \quad (23)$$

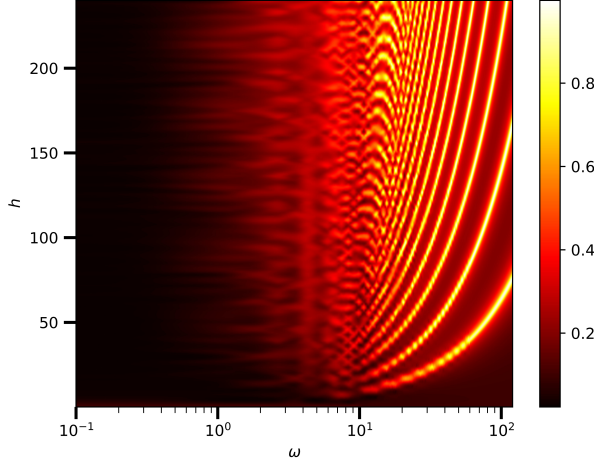


FIG. 3. Plot of the numerically averaged IPR (IPR computed using eqn 26) in the TSS plotted in the $h - \omega$ plane for $N = 100$ spins. In order to display the thermalized region more clearly, ω is plotted on a logarithmic scale on the abscissa. Note that, since the IPR is clearly non-negative, an average IPR of zero means that all Floquet states have zero IPR. Furthermore, the boundedness of IPR in $\phi_{IPR}(n) \leq 1$ ensures that if the average IPR is unity, then all Floquet states have unit IPR.

If ω is large enough to smooth out the harmonic components, we obtain the RWA,

$$\tilde{H}(t) \approx \tilde{H}_{\text{RWA}} \equiv -\frac{\hat{S}^2}{N-1} + \frac{(\hat{S}^x)^2}{N-1} - 2h_0\hat{S}^x - \frac{J_0(\eta)}{N-1} \left[(\hat{S}^z)^2 - (\hat{S}^y)^2 \right]. \quad (24)$$

If the drive amplitude h is adjusted such that η lies at a root of $J_0(\eta)$ (the localization point), the RWA Hamiltonian is diagonal in the representation of the simultaneous eigenstates of transverse field \hat{S}^x , and S^2 , yielding an IPR of unity in that representation, similar to the TFIM in the previous section. Note however, that if the DC transverse field h_0 is set to 0, then, at the localization point, the RWA Hamiltonian $\tilde{H}_{\text{RWA}} \sim (\hat{S}^x)^2$ in the TSS. The eigenvalues are two-fold degenerate. This produces infinitely many (Floquet) eigenmodes in the degenerate subspace whose IPRs may not always

be unity in the S^x representation. The removal of this degeneracy necessitates the inclusion of the d.c. field h_0 . However, note that rational values of h_0 may add accidental degeneracies in \tilde{H}_{RWA} . To see this, note that, at a localization point, the eigenvalues of \tilde{H}_{RWA} in the TSS are given by

$$\text{Eigs}[\tilde{H}_{\text{RWA}}] = \frac{\left(\frac{N}{2} - m\right)^2}{N-1} - 2h_0 \left(\frac{N}{2} - m\right), \quad (25)$$

where the half-integer $-N/2 \leq m \leq N/2$ is the eigenvalue corresponding to a particular eigenstate $|m\rangle$ of the symmetry-breaking field \hat{S}^x . In order to ensure that no additional degeneracies occur, we have to set h_0 in such a way that no two energies accidentally coincide. If $N \gg 1$ (substantially large), then this condition can be readily met by assuring that $(1 - 2h_0)^{-1}$ is never an integer that is divisible by N . To ensure this in our numerical simulations, we have kept h_0 at a small irrational value. The localization of the Floquet states at resonance is supported by exact numerical results, as can be seen in the phase diagram fig 3. Here, we have plotted the arithmetic mean over all Floquet states of the IPR in the TSS for each point in the $h - \omega$ plane for $N = 100$ spins. The IPR in S^x representation is

$$\phi_{IPR}(n) = \sum_m |\langle m | \phi^n \rangle|^4. \quad (26)$$

As can be readily seen in the figure, the IPR is essentially zero when $\omega \lesssim 1$. There is considerable structure in the phase diagram for larger drive frequencies, and along the lines given by the roots of $J_0(\eta)$, the IPR is essentially unity, in agreement with eqn. 24.

In figure 4, we show plots of the IPR of the Floquet modes $|\phi^n\rangle$ for $S^2 = (N/2)(N/2+1)$. These plots were obtained numerically by diagonalizing the propagator $U(t)$ at $t = T$, where $U(t)$ is defined in eqn 5. This propagator was obtained from simulations of the exact quantum dynamics using QuTiP, the Quantum Toolbox in Python [56]. We kept the frequency at a fairly large value $\omega = 90$ where we expect that RWA would be valid, and $N = \mathcal{O}(10^2)$. The density plot in the upper panel of fig 4 depicts the IPR of the Floquet states; the abscissa $\eta = 4h/\omega$ and the ordinate is $n/(2N+1)$, where $n \leq 2N$ is a non-negative integer

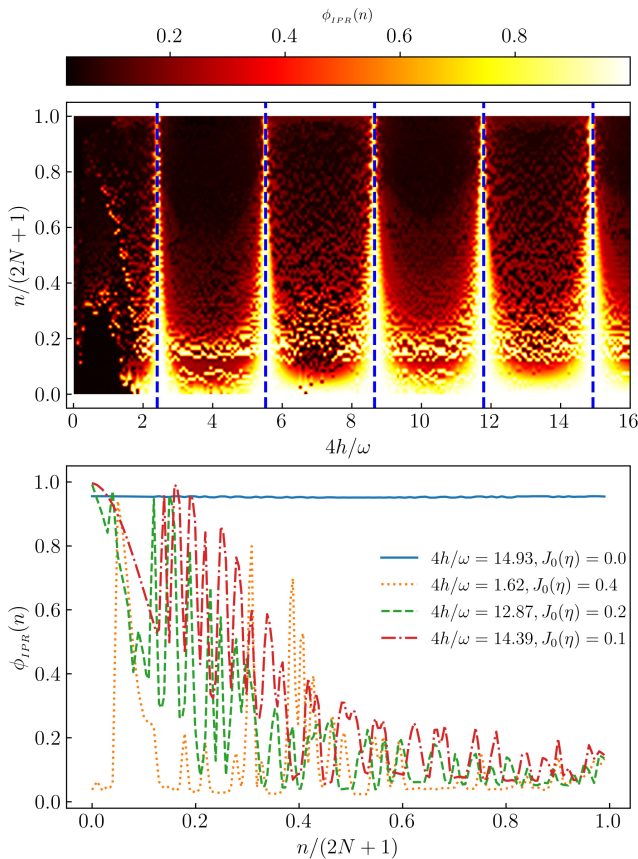


FIG. 4. IPR density plot for all possible Floquet modes (top panel ordinate) for different values of $\eta = 4h/\omega$ (top panel abscissa), deduced from equation 26 for exact LMG Hamiltonian for $N = 50$. Blue dashed lines are roots of $J_0(\eta)$. At bottom panel cross-section of IPR (ordinate)for four different η 's plotted for all possible floquet modes(bottom panel, abscissa) at $\omega = 90$. IPR founds to be \sim unity for all Floquet modes at roots of J_0 .

that indexes the Floquet states in increasing order of m . The dashed vertical lines correspond to the roots of $J_0(\eta)$. Comparing with the IPR of the TFIM in fig 1, we can see a very similar patterns in the immediate neighbourhood of the roots. Evidently, the IPR approaches a value of one for sufficiently large values of the roots, strongly suggesting full DMBL. Deviations occur at the smallest root of $J_0(\eta)$ (around $\eta = 2.405$) due to the contributions from higher order terms in eq 23. Thus, a higher root is favored for DMBL.

The bottom panel of fig 4 contains cross sections of the full IPR plot for selected values of η as indicated in the legend. When the drive amplitude h is adjusted such that η is close to a root of $J_0(\eta)$, the Floquet States are mixed, but not entirely thermal, since the IPR does not fall to $\mathcal{O}(N^{-1})$, indicating that localization persists to some extent. However, the further we are from the roots, the closer the IPR gets to one predicted by thermalization.

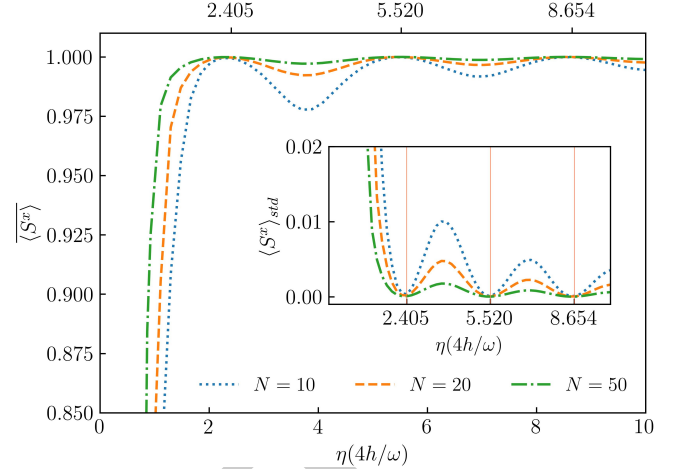


FIG. 5. Temporal average of $\langle \hat{S}^x \rangle$ (ordinate) for different η 's (abscissa) is plotted for $\sim 200T$ at higher ω for different $N=10, 20, 50$. $\langle \hat{S}^x \rangle$ is found to be unity at roots of $J_0(\eta)$. At points away from resonance points, $\langle \hat{S}^x \rangle$ falls below unity. The corresponding standard deviation $\langle \hat{S}^x \rangle_{std}$ supports the variation of $\langle \hat{S}^x \rangle$ (inset fig.). $\langle \hat{S}^x \rangle_{std}$ is ~ 0 describing a full freezing of the system at roots of $J_0(\eta)$ (red vertical solid lines).

Figure 5 shows plots of the long-time average (from $t = 0 - 200T$) of the field amplitude $\langle \hat{S}^x \rangle$ as a function of η . The system is started from the fully polarized state $s_n = N/2$ in the TSS and the dynamics simulated. The average is plotted for different values of amplitude h , keeping the frequency fixed at a high value of $\omega = 90$. It is clearly very close to unity at roots of $J_0(\eta)$ and falls at points away from it, indicating that S^x is approximately conserved at the localization points.

Small deviations do occur due to the role of higher order terms in the rotated Hamiltonian in eq 22. This can be demonstrated quantitatively by comparing the IPR obtained from the exact dynamics simulation with that obtained from the dynamics of $\tilde{H}(t)$ in eq. 22 after truncating the series at orders $k \geq 1$. This comparison can be seen in fig 6. The IPR plots from the exact dynamics indicate that the first localization point, represented by the lowest root of $J_0(\eta)$, does not show complete DMBL. However, DMBL is particularly conspicuous at large roots. The IPRs of the Floquet states obtained from the RWA dynamics exhibit large deviations from unity when away from the localization point as evidenced by the green and red curves in the middle panel of fig 6. However, complete localization is seen in the RWA dynamics at any localization point, in contrast to the exact case in the top panel. Thus, it is necessary to incorporate higher-order corrections into the Rotating Wave Approximation (RWA) at lower

449 III. PERSISTENCE OF DMBL IN THE CONTINUUM
450 LIMIT

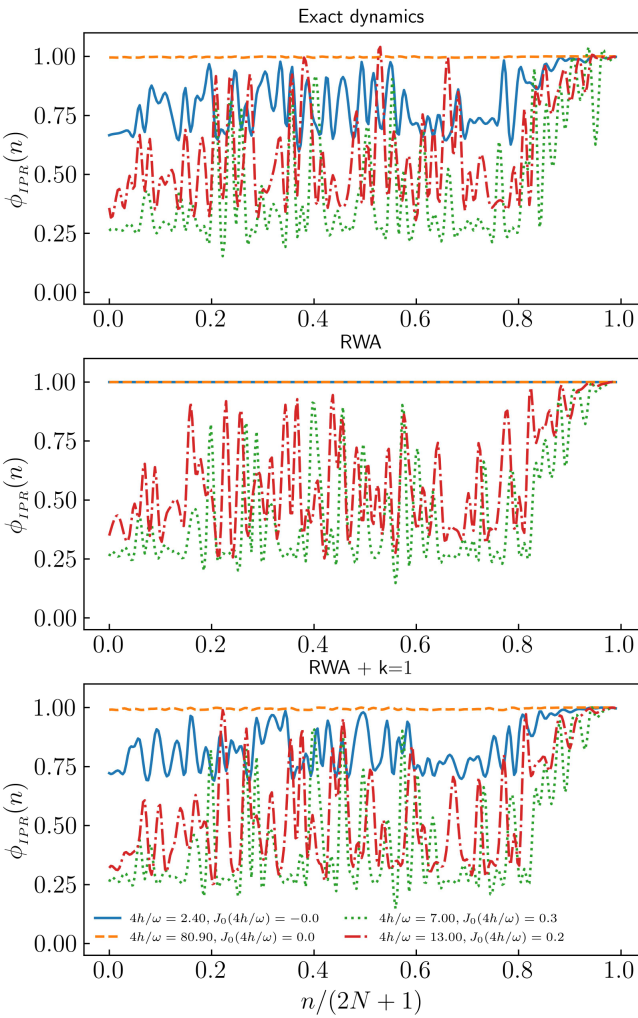


FIG. 6. The comparison between IPR for exact dynamics and RWA with corresponding correction orders. IPR is calculated for four different η 's and corresponding $J_0(\eta)$ values for colors, Blue : $\eta = 2.40, J_0(\eta) = 0.0$, dashed orange: $\eta = 80.9, J_0(\eta) = 0.0$, Green: $\eta = 7.0, J_0(\eta) = 0.3$, Red: $\eta = 13, J_0(\eta) = 0.2$. At low root of $J_0(\eta)$ IPR is not unity (Blue curve) while at higher root (orange dashed) it is unity while at points away from roots IPR are less than unity in the exact (top panel) plot. RWA does not matches with the exact plot. At all roots of $J_0(\eta)$ IPR is unity(middle panel). RWA with additional higher order terms exhibit similar system pattern(Bottom panel) with exact dynamics.

445 localization points. The application of the first-order
446 correction to RWA in the lower panel of fig 6 results in
447 a curve structure that is closer to that from the exact
448 dynamics.

451 In the continuum limit, where $N \rightarrow \infty$, the disparity
452 between neighboring values of s_i in equation 19 can
453 be disregarded, and s_i can be mapped to a continuum
454 $q \in [-1/2, 1/2]$ [55]. We define the Hamiltonian per
455 particle $h(t) \equiv \frac{H(t)}{N}$, and a canonically conjugate co-
456 ordinate $Np \equiv \left\langle -i \frac{\partial}{\partial q} \right\rangle$. Then, in this limit, the dynam-
457 ics can be approximated by that of a classical Hamil-
458 tonian [57]

$$h(t) = -2q^2 - [h \cos \omega t + h_0] \sqrt{1 - 4q^2} \cos p, \quad (27)$$

which yields the dynamical system

$$\begin{aligned} \frac{dq}{dt} &= \frac{\partial h}{\partial p} = h(t) \sqrt{1 - 4q^2} \sin p \\ \frac{dp}{dt} &= -\frac{\partial h}{\partial q} = 4q \left[1 - \frac{h(t) \cos p}{\sqrt{1 - 4q^2}} \right], \end{aligned} \quad (28)$$

459 where $h(t) = [h \cos \omega t + h_0]$. We have profiled simu-
460 lations of the ensuing dynamics with the *Poincaré sur-*
461 *face of section* (PSOS) of the full dynamics. Here, the
462 (q, p) -phase space is strobed at $t = nT$, and plotted
463 for a large number of initial conditions. The results
464 are shown in the upper panels of fig 7 for a small value
465 of $\omega = 2.0$ (left panel) and a large value $\omega = 90$ (right
466 panel). In both cases, the value of h is chosen such
467 that η lies on the first root of $J_0(\eta)$. The onset of chaos
468 for small drive frequency indicates thermal behaviour
469 for typical initial conditions, with small islands of reg-
470 ularity for others. This is consistent with similar re-
471 sults for small frequencies reported in [53, 58]. How-
472 ever, at high frequency, the regular islands distinctly
473 dominate over the chaos. The trajectories indicate
474 that the conservation of $\langle S^x \rangle \approx \sqrt{1 - 4q^2} \cos p$ [55]
475 at high ω persists in the thermodynamic limit. That
476 this is a signature of the underlying quantum dynam-
477 ics can be readily seen in the quantum phase space
478 representation of the Floquet Eigenstates for a large
479 but finite N . These are shown in the correspondingly
480 lower panels of fig 7. Here, we have plotted the Spec-
481 tral Average of the Husimi Q-functions of the acquired
482 Floquet States in the TSS. Specifically, for a coher-
483 ent state $|q, p\rangle$, the corresponding Spectral-Averaged
484 Husimi distribution [59] is obtained by

$$H(q, p) \equiv \frac{1}{(2N+1)\pi} \sum_n \langle q, p | \phi^n \rangle \langle \phi^n | q, p \rangle. \quad (29)$$

485 The quantum phase space retains signatures of the
486 classical phase space dynamics when $N = 100$, indi-
487 cating the onset of the persistence of S^x conservation
488 that arises from the resonance condition at high fre-
489 quencies.

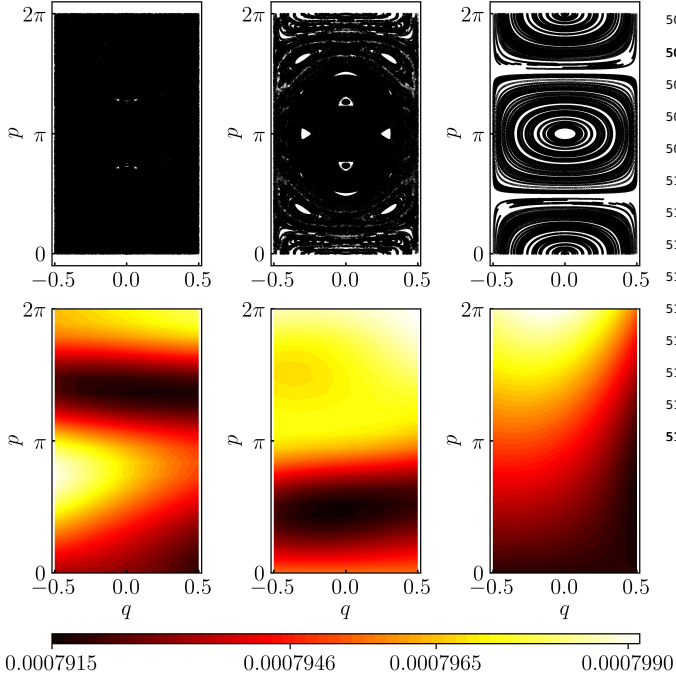


FIG. 7. Phase-space distributions at $\omega = 1.0$ (left panels), $\omega = 2.5$ (middle panels) and $\omega = 90.0$ (right panels) for 100 initial conditions. The drive amplitude h is always adjusted such that $\eta = 4h/\omega$ lies on the smallest root of $J_0(\eta)$, i.e. $\eta = 2.4048\dots$. At small $\omega = 1.0$, the classical PSOS, obtained from simulating the dynamics in eqns 28 (top left panel), shows chaotic behaviour, and at $\omega = 2.5$, regular regions start to appear. At higher $\omega = 90.0$, the dominance of regular dynamics can be readily seen (top right panel). The bottom panels plot the corresponding Spectral-Averaged Husimi-Q function, obtained from the Floquet modes $|\phi^n\rangle$ using eqn. 29, and setting $N = 100$. The $\omega = 1.0$ case (bottom left panel) has a dispersed distribution in colour. This is consistent with the chaotic behaviour seen in the continuum limit. At $\omega = 2.5$ (bottom middle panel), there is a partial regular pattern observed together with a dispersed pattern. In the $\omega = 90$ -case (bottom right panel), the distribution has distinct colour contrasts, which is consistent with the regular dynamics pattern seen in the continuum limit.

IV. PHASE CROSSOVER FROM THERMAL TO DMBL

The analysis of the periodically driven LMG model reveals two distinct scenarios at low and high external drive frequencies. In the former case, thermalization in accordance with FETH is seen, whereas in the latter case, DMBL is induced. As a result, we hypothesize that a macroscopic change in phase occurs due to the influence of frequency.

To demonstrate this, we investigate the IPR of the Floquet mode with smallest quasienergy for numerous frequencies and system sizes, along with the associated drive amplitude h keeping the system at a localization point. The results are shown in fig 8. In the

low-frequency range $\omega \in [1.0, 9.0]$, the IPR exhibits values well below unity. Moreover, the IPR gradually diminishes with increasing system size, following a system size inverse proportional trend, which confirms the participation distribution (as shown in the bottom panel). As the limit $N \rightarrow \infty$, the inverse participation ratio (IPR) tends towards zero, indicating a fully delocalized state. The plots reveal a gradual increase in the unity of IPR over a certain frequency range, specifically at $\omega \approx 5$. In addition, the rise does not cross with those for different values of N , suggesting the onset of a phase crossover [41, 60]. As the size of the system increases, the crossover region becomes smoother, rather than sharper.

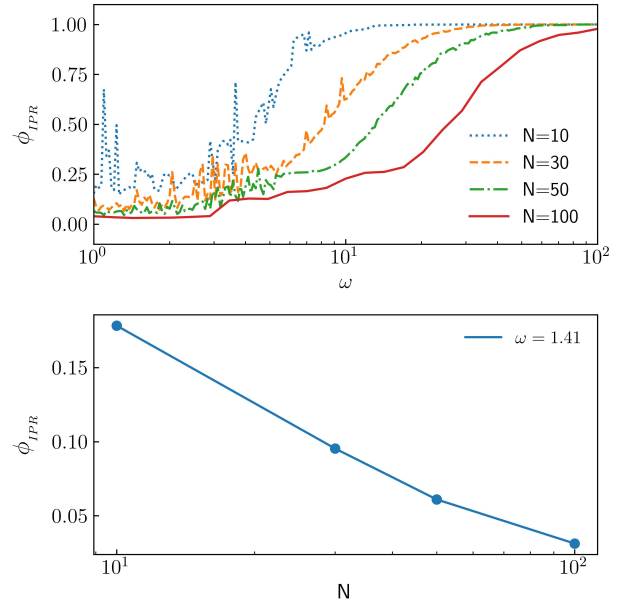


FIG. 8. IPR is plotted (top panel, ordinate) for a range of $\omega \in [1, 100]$ (top panel, abscissa) for four different $N = 10, 30, 50, 100$ at root of $J_0(\eta)$. At small ω upto $\omega \sim 10$ IPR founds to be very small and rises slowly upto unity (fully localized) at higher frequencies. At bottom panel IPR (ordinate) is plotted for different $N = 10, 30, 50, 100$ (bottom panel, abscissa) for a random small $\omega \sim 1$ at root of $J_0(\eta)$ from the values from top panel. IPR falls as inversely proportional to N , indicating an approach to a fully distributed (thermal) state. The smooth rise in IPR defines a phase crossover (top panel) between a fully thermal phase to a fully localized phase.

We can also look at this crossover more clearly in the plots of the heating rate of the system, defined simply by the expectation value of the Hamiltonian, $\langle \hat{H}(t) \rangle$. We have carried out the numerical evaluation from the simulated dynamics over $t = 500T$. When the system is adequately described by FETH, the temporal fluctuations in the heating-rate Hamiltonian, defined

How to identify the crossover frequency in the semiclassical? In fig. 7, it looks like conserved quantities appear at middle panel, $\omega = 2.5$, same place where IPR starts to rise in fig. 8. Is that good enough?

We're working on doing this thing outside the J_0 root.

529 by $\langle H \rangle_{std}^2 \equiv \overline{\langle \hat{H} \rangle^2} - \overline{\langle \hat{H} \rangle}^2$ (see eqn 3), are minimal in
 530 the thermodynamic limit, as the spread of states leads
 531 to a limited standard deviation[61]. Conversely, the
 532 onset of athermalism is indicated by nonzero fluctua-
 533 tions in time. If we set the initial state to the fully po-
 534 larized state in the TSS (given by $|s_N\rangle$), then the onset
 535 of freezing, together with DMBL, will result in nearly
 536 infinite hysteresis in the ensuing dynamics, causing
 537 $|\psi\rangle(t) \approx |s_N\rangle \forall t$. From eqn. 17, we can clearly see
 538 that this will lead to a linearly rising dependence on
 539 ω in $\langle H \rangle_{std}$ as long as we stick to a **localization point**
 540 given by a fixed h/ω [62]. All these observations are
 541 corroborated by the heating rate plots in figure 9.
 There is
 a new
 footnote.

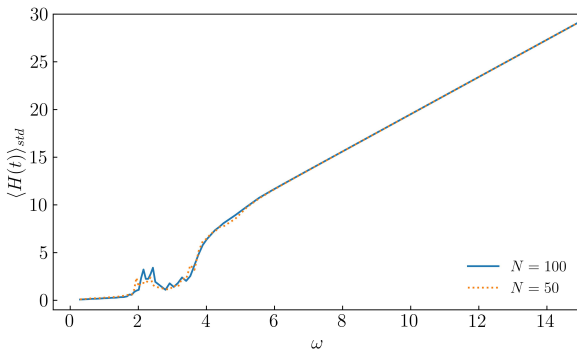


FIG. 9. The standard deviation of the heating rate, denoted by $\langle H \rangle_{std}$, calculated over a span of $t = 500T$ for two system sizes. Here, h is varied to keep $\eta = 4h/\omega$ at the first root of $J_0(\eta)$. A nonsingular rise has been identified at $\omega \approx 4.0$. $\langle H \rangle_{std}$ exhibits a diminutive magnitude below that value of ω , while a linear rise is observed at higher frequencies, consistent with freezing. A vanishingly small standard deviation for $\omega \ll 4.0$ indicates the presence of a thermal region, whereas a larger finite standard deviation suggests the existence of athermal behaviour. The small peaks observed at $\omega \in [2, 4]$ are finite-size effects that disappear in the thermodynamic limit.

543

544

545

V. CONCLUSION AND OUTLOOK

546 We have delved into the onset of freezing and
 547 phase cross-over in 1D spin systems driven by a time-
 548 periodic transverse field, contrasting the responses
 549 in the Transverse Field Ising Model (TFIM) with that
 550 of the long-range Lipkin-Meshkov-Glick Model (LMG).
 551 The parametrization of DMBL is based on the Inverse
 552 Participation Ratio (IPR) of the Floquet eigenstates.
 553 Our investigations compared the IPRs from both mod-
 554 els numerically, and found the emergence of thermal
 555 behavior at low frequencies and freezing at high fre-

556 quencies for the LMG model, the latter a direct conse-
 557 quence of the appearance of additional approximately
 558 conserved quantities.

559 Long-range spins exhibit strong localization in spin-
 560 coordinate space for the LMG model when the drive
 561 frequency is $\omega \gg J$, where J represents the spin ex-
 562 change energy. The localization of the LMG model
 563 occurs at specific resonance points of the drive fre-
 564 quency ω and amplitude h , at $J_0(4h/\omega) = 0$, $\omega \gg J$.
 565 This is apparently similar to the phenomenon of Dy-
 566 namical Freezing (DMF) in the Transverse Field Ising
 567 Model (TFIM), where comparable localization at res-
 568 onance points, determined by the roots of $J_0(2h/\omega)$,
 569 occurs due to the onset of an additional approximate
 570 conservation in the transverse field itself. However,
 571 a key difference is the thermal behaviour of the LMG
 572 model at low frequencies. Plots of the IPR for a range
 573 of frequencies along the resonance manifold exhibits
 574 a smooth increase in IPR yielding a quantum phase-
 575 crossover from a thermal phase governed by the Flo-
 576 quet Eigenstate Thermalization Hypothesis (FETH) to
 577 a Dynamically Many-Body localized phase (DMBL).
 578 This crossover is absent in the TFIM, as can be readily
 579 seen in the significant magnitude of the inverse par-
 580 ticipation ratio (IPR) even at low frequencies. Thus,
 581 the suppression of thermalization through Dynamical
 582 Many Body Localization in long-range systems can be
 583 controlled via Floquet engineering, even in clean sys-
 584 tems without any disorder. Thus, periodically driven
 585 long-range spin systems are an excellent tool for in-
 586 vestigating disorder-free Many Body Localization, as
 587 can be readily seen via the IPR of its Floquet modes.

588 There are several unexplored indicators of DMBL,
 589 such as entanglement entropy and level statistics [10],
 590 which we defer to future studies. In addition,
 591 Halpern in 2019 proposed a quantum engine based
 592 on MBL[11] which works between strong localized
 593 and thermal phases of the system. In our proposed
 594 LMG model, tuning the system parameters by bring-
 595 ing them to the resonance points, then adiabatically
 596 cycling the frequency from the thermal region to the
 597 DMBL region, can achieve a similar engine without
 598 going through a phase transition.

A. Acknowledgements:

600 One of the authors, MR acknowledges The Univer-
 601 sity of Burdwan for support via a state-funded fel-
 602 lowship. AR acknowledges support from the Uni-
 603 versity Grants Commission (UGC) of India, via BSR
 604 Startup Grant No. F.30-425/2018(BSR), as well as
 605 from the Science and Engineering Research Board
 606 (SERB) Core Research Grant No. CRG/2018/004002.

- [1] S. Bordia Pranjal, Lüschen Henrik, *Nature Physics* **13**, 460 (2017).
- [2] S. Sahoo, I. Schneider, and S. Eggert, Periodically driven many-body systems: A floquet density matrix renormalization group study (2019), arXiv:1906.00004 [cond-mat.str-el].
- [3] A. Das, *Phys. Rev. B* **82**, 172402 (2010).
- [4] G. B. Mbeng, A. Russomanno, and G. E. Santoro, The quantum ising chain for beginners (2020), arXiv:2009.09208 [quant-ph].
- [5] H. S. Yamada and K. S. Ikeda, *Phys. Rev. E* **105**, 054201 (2022).
- [6] A. Roy and A. Das, *Phys. Rev. B* **91**, 121106 (2015).
- [7] H. Li, B. Shapiro, and T. Kottos, *Phys. Rev. B* **98**, 121101 (2018).
- [8] A. Eckardt and E. Anisimovas, *New Journal of Physics* **17**, 093039 (2015).
- [9] L. Zhang, V. Khemani, and D. A. Huse, *Phys. Rev. B* **94**, 224202 (2016).
- [10] V. Khemani, A. Lazarides, R. Moessner, and S. L. Sondhi, *Phys. Rev. Lett.* **116**, 250401 (2016).
- [11] N. Yunger Halpern, C. D. White, S. Gopalakrishnan, and G. Refael, *Phys. Rev. B* **99**, 024203 (2019).
- [12] T. Nag, S. Roy, A. Dutta, and D. Sen, *Phys. Rev. B* **89**, 165425 (2014).
- [13] G. Carleo, F. Becca, M. Schiró, and M. Fabrizio, *Scientific Reports* **2**, 243 (2012).
- [14] S. Aditya and D. Sen, Dynamical localization and slow thermalization in a class of disorder-free periodically driven one-dimensional interacting systems (2023), arXiv:2305.06056 [cond-mat.stat-mech].
- [15] M. Schiulaz, A. Silva, and M. Müller, *Phys. Rev. B* **91**, 184202 (2015).
- [16] T. Grover and M. P. A. Fisher, **2014**, P10010.
- [17] Z. Papić, E. M. Stoudenmire, and D. A. Abanin, *Annals of Physics* **362**, 714 (2015).
- [18] A. Smith, J. Knolle, D. L. Kovrizhin, and R. Moessner, *Phys. Rev. Lett.* **118**, 266601 (2017).
- [19] O. Hart, S. Gopalakrishnan, and C. Castelnovo, *Phys. Rev. Lett.* **126**, 227202 (2021).
- [20] H. Lipkin, N. Meshkov, and A. Glick, *Nuclear Physics* **62**, 188 (1965).
- [21] N. Meshkov, A. Glick, and H. Lipkin, *Nuclear Physics* **62**, 199 (1965).
- [22] A. Glick, H. Lipkin, and N. Meshkov, *Nuclear Physics* **62**, 211 (1965).
- [23] P. Ribeiro, J. Vidal, and R. Mosseri, *Phys. Rev. E* **78**, 021106 (2008).
- [24] N. Debergh and F. Stancu, *Journal of Physics A: Mathematical and General* **34**, 3265 (2001).
- [25] P. Titum and M. F. Maghrebi, *Phys. Rev. Lett.* **125**, 040602 (2020).
- [26] A. Campa, T. Dauxois, and S. Ruffo, *Physics Reports* **480**, 57 (2009).
- [27] E. R. S. Eisele, *Theodor, Journal of Statistical Physics*, 161 (1988).
- [28] A. Canning, *Physica A: Statistical Mechanics and its Applications* **185**, 254 (1992).
- [29] D. Vu, K. Huang, X. Li, and S. Das Sarma, *Phys. Rev. Lett.* **128**, 146601 (2022).
- [30] G. Misguich, V. Pasquier, and J.-M. Luck, *Phys. Rev. B* **94**, 155110 (2016).
- [31] M. Calixto and E. Romera, *Journal of Statistical Mechanics: Theory and Experiment* **2015**, P06029 (2015).
- [32] K. Fujii, *Journal of Modern Physics* **8**, 2042 (2017).
- [33] D. A. Abanin, E. Altman, I. Bloch, and M. Serbyn, *Rev. Mod. Phys.* **91**, 021001 (2019).
- [34] M. Srednicki, *Phys. Rev. E* **50**, 888 (1994).
- [35] M. Srednicki, *Journal of Physics A: Mathematical and General* **32**, 1163 (1999).
- [36] M. Holthaus, *Journal of Physics B: Atomic, Molecular and Optical Physics* **49**, 013001 (2015).
- [37] M. Vogl, M. Rodriguez-Vega, and G. A. Fiete, *Phys. Rev. B* **101**, 024303 (2020).
- [38] M. Bukov, L. D'Alessio, and A. Polkovnikov, *Advances in Physics* **64**, 139 (2015).
- [39] L. D'Alessio and M. Rigol, *Phys. Rev. X* **4**, 041048 (2014).
- [40] R. Yousefjani, S. Bose, and A. Bayat, *Phys. Rev. Res.* **5**, 013094 (2023).
- [41] P. Sierant, M. Lewenstein, A. Scardicchio, and J. Zakrzewski, *Phys. Rev. B* **107**, 115132 (2023).
- [42] R. Yousefjani, S. Bose, and A. Bayat, *Phys. Rev. Res.* **5**, 013094 (2023).
- [43] F. Alet and N. Laflorencie, *Comptes Rendus Physique* **19**, 498 (2018).
- [44] S. J. Garratt and S. Roy, *Phys. Rev. B* **106**, 054309 (2022).
- [45] R. B. Stinchcombe, *Journal of Physics C: Solid State Physics* **6**, 2459 (1973).
- [46] F. E. H. George Arfken, Hans Weber, *Mathematical Methods for Physicists*, 7th ed. (Academic Press).
- [47] S. Mukherjee, A. Spracklen, D. Choudhury, N. Goldman, P. Öhberg, E. Andersson, and R. R. Thomson, *New Journal of Physics* **17**, 115002 (2015).
- [48] S.-H. Lin, B. Sbierski, F. Dorfner, C. Karrasch, and F. Heidrich-Meisner, *SciPost Phys.* **4**, 002 (2018).
- [49] N. C. Murphy, R. Wortis, and W. A. Atkinson, *Phys. Rev. B* **83**, 184206 (2011).
- [50] E. J. Torres-Herrera, I. Vallejo-Fabila, A. J. Martínez-Mendoza, and L. F. Santos, *Phys. Rev. E* **102**, 062126 (2020).
- [51] N. Trivedi and D. Heidarian, *Progress of Theoretical Physics Supplement* **160**, 296 (2005).
- [52] G. Misguich, V. Pasquier, and J.-M. Luck, *Phys. Rev. B* **94**, 155110 (2016).
- [53] A. Russomanno, R. Fazio, and G. E. Santoro, *Europhysics Letters* **110**, 37005 (2015).
- [54] N. Defenu, T. Enss, M. Kastner, and G. Morigi, *Phys. Rev. Lett.* **121**, 240403 (2018).
- [55] T. Mori, *Journal of Physics A: Mathematical and Theoretical* **52**, 054001 (2019).
- [56] J. Johansson, P. Nation, and F. Nori, *Computer Physics Communications* **184**, 1234.
- [57] B. Sciolla and G. Biroli, *Phys. Rev. Lett.* **105**, 220401 (2010).

- ⁷²³ [58] R. A. Kidd, M. K. Olsen, and J. F. Corney, Phys. Rev. A ⁷⁴³ [66] B. Marcos, A. Gabrielli, and M. Joyce, Open Physics **10**,
⁷²⁴ **100**, 013625 (2019). ⁷⁴⁴ 676.
- ⁷²⁵ [59] A. Bäcker, S. Fürstberger, and R. Schubert, Phys. Rev. ⁷⁴⁵ [67] A. Haldar and A. Das, Annalen der Physik **529**,
⁷²⁶ E **70**, 036204 (2004). ⁷⁴⁶ 1600333.
- ⁷²⁷ [60] S. Sachdev, *Quantum Phase Transitions*, 2nd ed. (Cam- ⁷⁴⁷ [68] J. M. Deutsch, Phys. Rev. A **43**, 2046 ().
⁷²⁸ bridge University Press, Cambridge, 2011). ⁷⁴⁸ [69] E. W. Hobson, On the Second Mean-Value Theorem of
⁷²⁹ [61] P. Reimann, Journal of Statistical Mechanics: Theory ⁷⁴⁹ the Integral Calculus (1909).
- ⁷³⁰ and Experiment **2021**, 103106 (2021).
- ⁷³¹ [62] When frozen, $|\psi(t)\rangle \approx |s_N\rangle$. From eqn 17, $\langle \hat{H}_{0,1} \rangle$ are ⁷⁵⁰ [70] M. Rigol and M. Srednicki, Physical Review Letters
⁷³² both approximately constant. Averaging the square of ⁷⁵¹ **108**, 10.1103/physrevlett.108.110601 (2012).
- ⁷³³ $\langle \hat{H}(t) \rangle$ over long times $\tau \gg T$ yields a result that goes ⁷⁵² [71] J. M. Deutsch, IOP Publishing Ltd **81**, 296 ().
- ⁷³⁴ as $h^2 + \delta$, where $\delta \sim h_0 \ll 1$. Thus, the standard devia- ⁷⁵³ [72] R. Nandkishore and D. A. Huse, Annual Re-
⁷³⁵ tion in time will go as $\sim h \sim \omega$, since $\eta = 4h/\omega$ is kept ⁷⁵⁴ view of Condensed Matter Physics **6**, 15 (2015),
⁷³⁶ fixed. ⁷⁵⁵ <https://doi.org/10.1146/annurev-conmatphys-031214-014726>.
- ⁷³⁷ [63] L. Reichl, *The Transition to Chaos: Conservative Clas- ⁷⁵⁶ [73] L. D'Alessio and A. Polkovnikov, **333**, 19.*
- ⁷³⁸ sical and Quantum Systems, Fundamental Theories of ⁷⁵⁷ [74] S. Notarnicola, F. Iemini, D. Rossini, R. Fazio, A. Silva,
⁷³⁹ Physics, Vol. 200 (Springer International Publishing). ⁷⁵⁸ and A. Russomanno, Phys. Rev. E **97**, 022202 (2018).
- ⁷⁴⁰ [64] N. Srivatsa, R. Moessner, and A. E. Nielsen, Phys. Rev. ⁷⁵⁹ [75] A. Lazarides, A. Das, and R. Moessner, Phys. Rev. Lett. ⁷⁶⁰ **115**, 030402 (2015).
- ⁷⁴¹ Lett. **125**, 240401.
- ⁷⁴² [65] Quantum ising phase transition.